PAPER

Cattaneo-Christov Double Diffusion (CCDD) and magnetized stagnation point flow of non-Newtonian fluid with internal resistance of particles

IOP Publishing Physica Scripta
Phys. Scr. 95 (2020) 125002 (10pp) https://doi.org/10.1088/1402-4896/abc0c2

Cattaneo-Christov Double Diffusion (CCDD) and magnetized stagnation point flow of non-Newtonian fluid with internal resistance of particles

M Ijaz Khan[1] **and Faris Alzahrani**[2]

[1] Department of Mathematics and Statistics, Riphah International University I-14, Islamabad 44000, Pakistan
[2] Nonlinear Analysis and Applied Mathematics (NAAM)-Research Group, Department of Mathematics, Faculty of Sciences, King Abdulaziz University, PO Box 80203, Jeddah 21589, Saudi Arabia

E-mail: ijazfmg_khan@yahoo.com

Received 2 September 2020
Accepted for publication 13 October 2020
Published 29 October 2020

Abstract

Intention here is to discuss the physical features of MHD stagnation point flow of Williamson nanomaterial over a stretched surface. Cattaneo-Christov Double Diffusion (CCDD) concept is incorporated to deliberate the behaviors of mass and heat transfer rates. These models are based upon Fick's and Fourier's laws versus solutal and thermal relaxation times. Innovative characteristics regarding thermophoresis and Brownian diffusion effect are also scrutinized. Relevant transformations are used to reduce the nonlinear expression to ordinary one. Convergent solution by optimal homotopy analysis technique (OHAM) is constructed. The average residual error is computed through OHAM Discussion is arranged for velocity, concentration and temperature. Skin friction co-efficient, temperature gradient and mass transfer rate are graphically discussed. Velocity boosts up significantly via velocity ratio parameter. Temperature and velocity have opposite effects for Weissenberg number. Concentration of the material particles increases against larger estimations of thermal relaxation time.

Keywords: Williamson fluid model, Cattaneo-Christov double diffusion (CCDD), porous medium, viscous dissipation, magnetohydrodynamics, Brownian and thermophoresis diffusions

(Some figures may appear in colour only in the online journal)

1. Introduction

The applications of heat and mass transportation is increased recently due to various industrial and engineering processes, like heat exchanger, refrigeration, biomedical applications, air conditioning, food processing, damage of crops etc. Until now numerous investigators for mass and heat, transportation used convectional transport theories. Such theories are not reliable because of infinite speed of wave transmission. To overcome such inefficiency the solutal and thermal relaxation times are invoked. Initially, Cattaneo [1] made a development in Fourier's law by addition of thermal relaxation time and thus heat is conveyed in realistic pattern. Cattaneo-Christov mass and heat flux model was modified to scrutinize the behavior of thermal and solutal aspects in heat and mass transfer. Recently, various investigators developed Fick's and Fourier's laws to discourse stress relaxation in concentration and temperature distributions. Impact of variable thermal conductivity on Maxwell liquid flow with Cattaneo-Christov heat flux by a stretching sheet is explored by Hayat *et al* [2]. In this research work, they used Cattaneo-Christov heat flux instead of Fourier's law of heat conduction. The nonlinear flow equations are first altered into ordinary ones and then series solutions are obtained by the help of homotopy analysis method. The salient behavior of heat source/sink in Williamson nanofluid flow is exemplified by Khan *et al* [3]. The

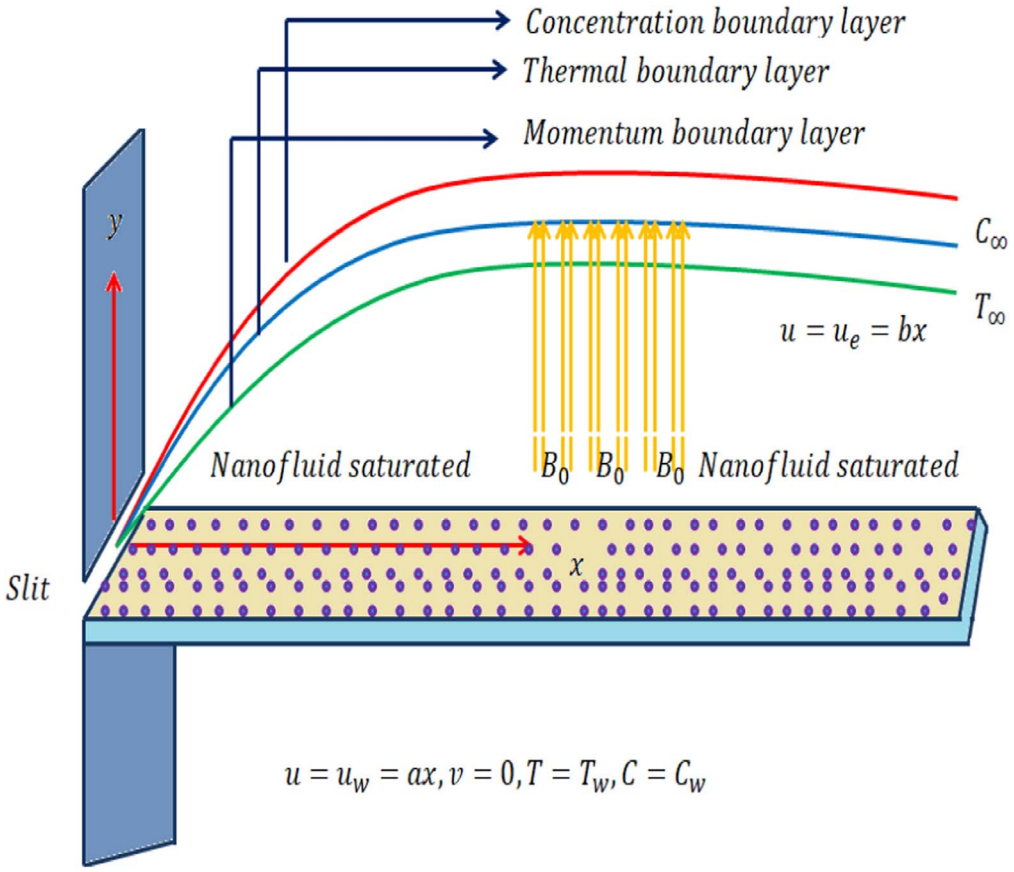

Figure 1. Flow diagram.

flow phenomenon is carried out over an oscillatory stretched surface. Furthermore, heat source/sink and convective boundary conditions for both heat and mass transport are implemented at the boundary. Their results indicated that the heat transfer rate is more subject to the insertion of nanoparticles. Zhang *et al* [4] reported the effect of relaxation-retardation dissipation in time dependent Oldroyd-B liquid flow with Cattaneo-Christov mass and heat fluxes. In this work, they discussed the thin film liquid flow towards a time dependent stretched surface. Furthermore, the energy equation is discussed and developed in the presence of viscous dissipation and CCDD theory. The nonlinear governing expressions are tackled by a new well-organized analytical technique called Double Parameter Transformation Expansion Method. Their valuable outcomes highlights that film thickness boosts versus higher values of unsteadiness parameter in case $\beta_2 > \beta_1$ while it thickness decrease for $\beta_2 < \beta_1$. Cattaneo-Christov double diffusion in squeezing the flow of a viscous fluid with concentration dependent mass diffusivity in a Darcy medium is highlighted by Farooq *et al* [5]. In this research work, Farooq *et al* again discuss the Cattaneo-Christov theory in fluid flow, but this time they used squeezing flow instead of steady flow and the results are calculated via same method as discussed in Ref. [2]. Waqas *et al* [6] examined the variable thermal conductivity in Powell-Eyring fluid flow by a stretchable cylinder. In this research work main consideration is given to the skin friction coefficient and discussed subject to various embedded variables. The results interprets that both concentration and temperature distributions are decreasing functions of concentration and thermal relaxation time respectively. Characteristics of Cattaneo-Christov flux in Jeffrey liquid flow of variable conductivity is examined by Hayat *et al* [7]. This work based on the following fourfold (i): Variable thermal conductivity (ii): Variable thicked surface (iii): Double stratification (iv): Nonlinear stretching phenomenon. Upadhay *et al* [8] discussed the Cattaneo-Christov mass and heat fluxes in time-dependent magnetohydrodynamic Eyring Powell liquid flow. Their calculated outcomes shows that the behavior of thermal relaxation is more in liquid phase than the dust phase subject to both PWT and PHF and also prescribed heat flux case. Hayat *et al* [9] reported the Jeffrey liquid flow with Cattaneo-Christov mass and heat fluxes. It is examined that the curves of velocity field diminishes against higher ratio of relaxation to retardation time. The temperature field decays subject to rising thermal relaxation parameter, Prandtl number and Deborah number. Malik *et al* [10] discussed the thermal heat flux in Sisko liquid flow with Cattaneo-Christov double diffusion. The governing equations are first altered into first order ordinary ones and then computational results are carried out through Shooting technique along with Runge–Kutta method (Fourth order).

Nanomaterial is a nano-size solid particles (1–100 nm) suspended in traditional fluids [11, 12]. Such liquids possess higher effect in the growth of pioneering heat conveyance fluids and extensive attempts was accomplished in this

direction during the last few decades. Nanoliquids have various applications in different fields of advanced industries, nano-electronics and nanotechnology containing military goods, micro manufacturing, desalination of water, microelectronic device technologies, carbon nanotubes, nuclear reactors chilling and silver nanoparticles in food packaging. Furthermore this modern-day technology is responsible for new opportunities to enhance the rate of heat conduction in different industrial processes. The model deliberated by Buongiorno [13] has achieved more attention subsequently it importantly describes the conduction mechanism between base liquid and nanoparticles. The behavior of thermophoresis and Brownian diffusion in third grade nanoliquids with binary chemical reaction is examined by Hayat *et al* [14]. Some recent attempts which discuss the characteristics of viscous and non-Newtonian material in fluid flow [15–25].

In the current study, we investigate the behavior of MHD stagnation point flow of Williamson nanomaterials. Mass and heat, transportation behaviors are scrutinized through Cattaneo-Christov mass and heat flux models. These models are the development of the laws of Fick's and Fourier's with a solutal and thermal relaxation time. The applied magnetic field is considered. Impact of Brownian movement and thermophoresis are accounted. The transformation procedure gives rise to an ordinary differential system. For convergent series solution the system is solved by OHAM [26–30]. Graphical representations for velocity, temperature and concentration are discussed. Furthermore, heat transfer rate, gradient of velocity and concentration gradients are also examined.

The main goal of the present research work is threefold. (i) Cattaneo-Christov Double Diffusion (CCDD) modeling with nanofluid for Williamson fluid is developed. (ii) The modeling of MHD and nanofluid with CCDD in implicit form is calculated for such fluid. (iii) Correct form of viscous dissipation and slip mechanisms like Brownian motion and thermophoretic diffusion is introduced first time in the literature.

The remaining manuscript is arranged as: The valuable review about the topic is displayed in 1, coordinate system and modeling is highlighted in 2, engineering interest is elaborated in 3, solution methodology is presented in 4, convergence of nonlinear flow expressions is outlined in 5, discussion of pertinent parameters are discussed and presented graphically in 6 and the final meaningful remarks are listed in 7.

2. Formulation

Here the MHD stagnation point flow of Williamson nanomaterials towards a stretching surface is considered. Brownian motion and thermophoresis are addressed. Cattaneo-Christove mass and heat flux models are used. Stretching surface is parallel to $x-$ direction. Clearly $y-$ axis is normal to the surface. The figure 1 depicts the schematic flow diagram of the present problem.

The magnetic field of constant strength (B_0) is exerted. The Joule heating is ignored in this research work due to week magnetic force due to which small amount of heat produced in the working fluid. Therefore, we ignore the Joule heating effect in the energy equation. Let $u = ax$ denotes stretching velocity and $u \to u_e = bx$ the free stream velocity where the constants a and b has dimensions of $1/\text{time}$.

The flow, temperature and concentration expressions satisfy

$$\frac{\partial u}{\partial x} + \frac{\partial v}{\partial y} = 0, \tag{1}$$

$$u\frac{\partial u}{\partial x} + v\frac{\partial u}{\partial y} = \nu_f \frac{\partial^2 u}{\partial y^2} + \sqrt{2}\,\nu_f \Gamma \frac{\partial u}{\partial y}\frac{\partial^2 u}{\partial y^2} - \frac{\sigma B_0^2}{\rho}(u - u_e) + u_e \frac{du_e}{dx}, \tag{2}$$

$$\left.\begin{aligned} &u\frac{\partial T}{\partial x} + v\frac{\partial T}{\partial y} + \frac{\mu_f}{(\rho c_p)_f}\left[\left(\frac{\partial u}{\partial y}\right)^2 + \Gamma\left(\frac{\partial u}{\partial y}\right)^3\right] \\ &- \tau D_B \delta_E\left(u\frac{\partial C}{\partial y}\frac{\partial^2 T}{\partial x \partial y} + u\frac{\partial T}{\partial y}\frac{\partial^2 C}{\partial x \partial y} + v\frac{\partial C}{\partial y}\frac{\partial^2 T}{\partial y^2} + v\frac{\partial T}{\partial y}\frac{\partial^2 C}{\partial y^2}\right) \\ &\delta_E\left(u\frac{\partial u}{\partial x}\frac{\partial T}{\partial x} + v\frac{\partial v}{\partial y}\frac{\partial T}{\partial y} + u^2\frac{\partial^2 T}{\partial x^2} + v^2\frac{\partial^2 T}{\partial y^2}\right. \\ &\left. + 2uv\frac{\partial^2 T}{\partial x \partial y} + u\frac{\partial v}{\partial x}\frac{\partial T}{\partial y} + v\frac{\partial u}{\partial y}\frac{\partial T}{\partial x}\right) \\ &- 2\tau\frac{D_T}{T_\infty}\delta_E\left(u\frac{\partial T}{\partial y}\frac{\partial^2 T}{\partial x \partial y} + v\frac{\partial T}{\partial y}\frac{\partial^2 T}{\partial y^2}\right) \\ &+ 2\mu\delta_E\left(u\frac{\partial^2 v}{\partial x^2} + v\frac{\partial^2 v}{\partial y^2}\right) = \frac{k}{(\rho c_p)_f}\left(\frac{\partial^2 T}{\partial y^2}\right) \\ &+ \tau D_B\left(\frac{\partial T}{\partial y}\frac{\partial C}{\partial y}\right) + \tau\frac{D_T}{T_\infty}\left(\frac{\partial T}{\partial y}\right)^2 \end{aligned}\right\}, \tag{3}$$

$$\left.\begin{aligned} &u\frac{\partial C}{\partial x} + v\frac{\partial C}{\partial y} + \delta_C\left(u\frac{\partial u}{\partial x}\frac{\partial C}{\partial x} + v\frac{\partial v}{\partial y}\frac{\partial C}{\partial y} + u^2\frac{\partial^2 C}{\partial x^2} + v^2\frac{\partial^2 C}{\partial y^2}\right. \\ &\left. + 2uv\frac{\partial^2 C}{\partial x \partial y} + u\frac{\partial v}{\partial x}\frac{\partial C}{\partial y} + v\frac{\partial u}{\partial y}\frac{\partial C}{\partial x}\right) \\ &- \frac{D_T}{T_\infty}\delta_C\left(u\frac{\partial^3 T}{\partial x \partial y} + v\frac{\partial^3 T}{\partial y^3}\right) = D_B\frac{\partial^2 C}{\partial y^2} + \frac{D_T}{T_\infty}\frac{\partial^2 T}{\partial y^2} \end{aligned}\right\}, \tag{4}$$

with

$$\left.\begin{aligned} &u = ax,\ v = 0,\ T = T_w,\ C = C_w \text{ at } y = 0, \\ &u = bx,\ T = T_\infty C = C_\infty \text{ when } y \to \infty. \end{aligned}\right\} \tag{5}$$

Here ρ_f symbolizes the density, u, v the velocity components, ν_f the kinematic viscosity, μ_f the dynamic viscosity, x, y the Cartesian coordinates Γ the Williamson liquid parameter, c_p the specific heat, σ the electrical conductivity, δ_E the thermal relaxation time, τ the ratio between heat capacities, D_B the Brownian movement coefficient, T the temperature, T_w the wall temperature, T_∞ the ambient temperature respectively, k the thermal conductivity, D_T the coefficient of thermophoresis, C the concentration, C_w the wall concentration, C_∞ the ambient concentration and δ_C the relaxation time of mass flux.

Taking

$$\left.\begin{aligned} u = axf'(\eta),\ v = -\sqrt{a\nu_f}f(\eta),\ \theta(\eta) = \tfrac{T-T_\infty}{T_w-T_\infty},\\ \phi(\eta) = \tfrac{C-C_\infty}{C_w-C_\infty},\ \eta = \sqrt{\tfrac{a}{\nu_f}}y \end{aligned}\right\} \quad (6)$$

we obtain

$$f''' + Wef''f''' - f'^2 + ff'' - Mf' + A^2 + MA = 0, \quad (7)$$

$$\left.\begin{aligned} &\theta'' + \mathrm{Pr}f\theta' + \mathrm{Pr}(Nb\theta'\phi' + Nt\theta'^2)\\ &+ Br\left(f'^2 + \tfrac{We}{\sqrt{2}}f'^3\right) - \mathrm{Pr}\beta_e(ff'\theta' + f^2\theta'')\\ &- \mathrm{Pr}\beta_e Nb(f\theta''\phi' + f\theta'\phi'') + 2\beta_e Ntf\theta'\theta''\\ &- 2Br\beta_e(f'f'^2 - ff''f''') = 0, \end{aligned}\right\}, \quad (8)$$

$$\phi'' + \mathrm{Pr}Le\beta_c f\phi' + \frac{Nt}{Nb}\theta'' - \mathrm{Pr}LeC(ff'\phi' + f^2\phi'') - \beta_c\frac{Nt}{Nb}f\theta\theta'' = 0, \quad (9)$$

$$\left.\begin{aligned} f(0) = 0, f'(0) = 1,\ \theta(0) = 1,\ \phi(0) = 1,\\ f'(\infty) = A,\ \theta(\infty) = 0,\ \phi(\infty) = 0, \end{aligned}\right\} \quad (10)$$

In the above expressions $We\left(=\frac{\Gamma a^{3/2}\sqrt{2}}{\nu_f^{1/2}}\right)$ denotes the Weissenberg number, $A\left(=\frac{b}{a}\right)$ the ratio parameter, $M\left(=\frac{\sigma B_0^2}{a\rho_f}\right)$ the magnetic parameter, $\beta_e(=a\delta_E)$ thermal relaxation time parameter, $\mathrm{Pr}\left(=\frac{\nu_f}{\alpha_f}\right)$ the Prandtl number, $Nb\left(=\frac{\tau D_B(C_w-C_\infty)}{\nu_f}\right)$ the Brownian motion parameter, $Ec\left(=\frac{u_w^2}{(c_p)_f(T_w-T_\infty)}\right)$ the Eckert number, $Nt\left(=\frac{\tau D_T(T_w-T_\infty)}{\nu_f T_\infty}\right)$ the thermophoresis parameter, $Br(=\mathrm{Pr}.Ec)$ the Brinkman number, $\beta_c(=a\delta_C)$ solutal relaxation time parameter and $Le\left(=\frac{\alpha}{D_B}\right)$ the Lewis number.

3. Engineering quantities

3.1. Coefficient of skin friction

Skin friction coefficient obeys

$$C_{fx} = \frac{\tau_w|_{z=0}}{\rho_f u_w^2}, \quad (11)$$

in which τ_w satisfies

$$\tau_w = \mu\left[\frac{\partial u}{\partial y} + \frac{\Gamma}{2}\left(\frac{\partial u}{\partial y}\right)^2\right]\Bigg|_{y=0}, \quad (12)$$

The above two expression lead to the following results

$$\sqrt{2}\,C_{fx}Re_x^{1/2} = f''(0) + Wef''(0)^2. \quad (13)$$

4. Solutions methodology

Initial approximation and linear operators are selected as follows

$$\left.\begin{aligned} f_0(\eta) = 1 - e^{-\eta} + A(\eta - 1 + e^{-\eta}),\\ \theta_0(\eta) = e^{-\eta}\\ \phi_0(\eta) = e^{-\eta}, \end{aligned}\right\} \quad (14)$$

$$\left.\begin{aligned} L_f = \frac{\partial^3}{\partial\eta^3} - \frac{\partial}{\partial\eta},\\ L_\theta = \frac{\partial^2}{\partial\eta^2} - 1,\\ L_\phi = \frac{\partial^2}{\partial\eta^2} - 1, \end{aligned}\right\} \quad (15)$$

liner operators have properties

$$\left.\begin{aligned} L_f = [a_0 + a_1e^{\eta} + a_3e^{-\eta}],\ L_\theta = [a_4e^{\eta} + a_5e^{-\eta}],\\ L_\phi = [a_6e^{\eta} + a_7e^{-\eta}], \end{aligned}\right\} \quad (16)$$

in which $a_i(i = 1,\ 2,\ 3,..., 7)$ denotes the arbitrary constants.

Let us assume that $\hbar_f$, $\hbar_g$ and $\hbar_\theta$ the auxiliary parameters and q an embedding variable $q \in [0,\ 1]$ then the zeroth order deformation problems can be expressed as follow:

$$(1-p)\,\mathbf{L}_1[F(\eta;\ p) - f_0(\eta)] = p\hbar_f\Re_f\mathbf{L}_f[F(\eta;\ p)], \quad (15)$$

$$(1-p)\,\mathbf{L}_2[\theta(\eta;\ p) - \theta_0(\eta)] = p\hbar_\theta\Re_\theta\mathbf{L}_\theta[\theta(\eta;\ p)], \quad (16)$$

$$(1-p)\,\mathbf{L}_3[\phi(\eta;\ p) - \phi_0(\eta)] = p\hbar_\phi\Re_\phi\mathbf{L}_\phi[\phi(\eta;\ p)], \quad (17)$$

$$\left.\begin{aligned} F'(0;\ p) = 1,\ F(0;\ p) = 0,\ F'(\infty;\ p) = A,\ \theta(0;\ p) = 1,\\ \theta(\infty;\ p) = 0,\ \phi(0;\ p) = 1,\ \phi(\infty;\ p) = 0. \end{aligned}\right\} \quad (18)$$

$$\left.\begin{aligned} \mathbf{L}_f = \tfrac{\partial^3F(\eta;\ p)}{\partial\eta^3} + We\tfrac{\partial^2F(\eta;\ p)}{\partial\eta^2}\tfrac{\partial^3F(\eta;\ p)}{\partial\eta^3} + F(\eta;\ p)\tfrac{\partial^2F(\eta;\ p)}{\partial\eta^2}\\ - \left(\tfrac{\partial F(\eta;\ p)}{\partial\eta}\right)^2 - M\left(\tfrac{\partial F(\eta;\ p)}{\partial\eta}\right) - \beta\left(\tfrac{\partial F(\eta;\ p)}{\partial\eta}\right)\\ A^2 + MA + \beta A, \end{aligned}\right\} \quad (19)$$

$$\left.\begin{aligned} \mathbf{L}_\theta = \tfrac{\partial^2\theta(\eta;\ p)}{\partial\eta^2} + \mathrm{Pr}\left(F(\eta;\ p)\tfrac{\partial\theta(\eta;\ p)}{\partial\eta}\right) + Br\left(\tfrac{\partial^2F(\eta;\ p)}{\partial\eta^2}\right)^2\\ + \tfrac{BrWe}{\sqrt{2}}\left(\tfrac{\partial^2F(\eta;\ p)}{\partial\eta^2}\right)^3 + 2Br\beta_eF(\eta;\ p)\tfrac{\partial^2F(\eta;\ p)}{\partial\eta^2}\tfrac{\partial^3F(\eta;\ p)}{\partial\eta^3}\\ - 2Br\beta_e\left(\tfrac{\partial F(\eta;\ p)}{\partial\eta}\right)\left(\tfrac{\partial^2F(\eta;\ p)}{\partial\eta^2}\right)^2\\ - \mathrm{Pr}\beta_e\left(\left(F(\eta;\ p)\tfrac{\partial F(\eta;\ p)}{\partial\eta}\tfrac{\partial\theta(\eta;\ p)}{\partial\eta}\right)\right.\\ \left. - \left(F(\eta;\ p)\tfrac{\partial^2F(\eta;\ p)}{\partial\eta^2}\tfrac{\partial^3F(\eta;\ p)}{\partial\eta^3}\right)\right)\\ - \mathrm{Pr}\beta_eNt\left(\left(F(\eta;\ p)\tfrac{\partial^2\phi(\eta;\ p)}{\partial\eta^2}\tfrac{\partial\phi(\eta;\ p)}{\partial\eta}\right)\right.\\ \left. + \left(F(\eta;\ p)\tfrac{\partial^2\theta(\eta;\ p)}{\partial\eta^2}\tfrac{\partial\phi(\eta;\ p)}{\partial\eta}\right)\right) \end{aligned}\right\} \quad (20)$$

$$\left.\begin{aligned}\mathbf{L}_{\phi} &= \frac{\partial^2\phi(\eta;\ p)}{\partial\eta^2} + \mathrm{Pr}Le\left(F(\eta;\ p)\frac{\partial\phi(\eta;\ p)}{\partial\eta}\right)\\ &- \beta_c\frac{Nt}{Nb}\left(F(\eta;\ p)\frac{\partial^2\theta(\eta;\ p)}{\partial\eta^2}\right) + \frac{Nt}{Nb}\left(\frac{\partial\theta(\eta;\ p)}{\partial\eta}\right)^2\\ &\mathrm{Pr}Le\beta\left(\left((F(\eta;\ p))^2\frac{\partial^2F\phi(\eta;\ p)}{\partial\eta^2}\right)_c\right.\\ &\left.+\left(F(\eta;\ p)\frac{\partial F(\eta;\ p)}{\partial\eta}\frac{\partial\phi(\eta;\ p)}{\partial\eta}\right)\right)\end{aligned}\right\} \quad (21)$$

Deformation problem for m[th] order are

$$\mathbf{L}_1[f_m - \chi_m f_{m-1}] = \hbar_f R_m^f, \quad (22)$$

$$\mathbf{L}_2[\theta_m - \chi_m\theta_{m-1}] = \hbar_\theta R_m^\theta, \quad (23)$$

$$\mathbf{L}_2[\phi_m - \chi_m\phi_{m-1}] = \hbar_\phi R_m^\phi, \quad (24)$$

$$\left.\begin{aligned}\left.\frac{\partial f_m}{\partial\eta}\right|_{\eta=0} = f_m|_{\eta=0} &= \left.\frac{\partial f_m}{\partial\eta}\right|_{\eta=\infty} = 0,\\ \left.\frac{\partial\theta_m}{\partial\eta}\right|_{\eta=0} &= \theta_m|_{\eta=\infty} = 0,\\ \left.\frac{\partial\phi_m}{\partial\eta}\right|_{\eta=0} &= \phi_m|_{\eta=\infty} = 0,\end{aligned}\right\} \quad (25)$$

in which

$$\left.\begin{aligned}R_m^f &= f_{m-1}''' + We\sum_{k=0}^{m-1} f_{m-1-k}'' f_k''' - \sum_{k=0}^{m-1} f_{m-1-k}' f_k'\\ &+ \sum_{k=0}^{m-1} f_{m-1-k} f_k'' - Mf_{m-1}' - \beta f_{m-1}'\\ &+ A^2(1-\chi_m) + MA(1-\chi_m) + \beta A(1-\chi_m),\end{aligned}\right\} \quad (21)$$

$$\left.\begin{aligned}R_m^\theta &= \theta_{m-1}'' + \mathrm{Pr}\sum_{k=0}^{m-1} f_{m-1-k}\theta_k' + \mathrm{Pr}Nb\sum_{k=0}^{m-1}\theta_{m-1-k}'\varphi_k'\\ &+ \mathrm{Pr}Nt\sum_{k=0}^{m-1}\theta_{m-1-k}'\theta_k'\\ &+ Br\frac{We}{\sqrt{2}}\sum_{k=0}^{m-1} f_{m-1-k}'' f_{k-1}'' f_k'' - \mathrm{Pr}\beta_e\sum_{k=0}^{m-1} f_{m-1-k} f_{k-1}'\theta_k'\\ &- \mathrm{Pr}\beta_e\sum_{k=0}^{m-1} f_{m-1-k} f_{k-1}\theta_k''\\ &+ 2\beta_e Nt\sum_{k=0}^{m-1} f_{m-1-k}\theta_{k-1}'\theta_k''\\ &- \mathrm{Pr}\beta_e Nb\sum_{k=0}^{m-1}(f_{m-1-k}\theta_{k-1}''\varphi_k' + f_{m-1-k}\theta_{k-1}'\varphi_k'')\\ &+ Br\sum_{k=0}^{m-1} f_{m-1-k}'' f_k''\\ &- 2Br\beta_e\sum_{k=0}^{m-1}(f_{m-1-k} f_{k-1}'' f_k'' - f_{m-1-k} f_{k-1}'' f_k'''),\end{aligned}\right\} \quad (22)$$

$$\left.\begin{aligned}R_m^\phi &= \phi_{m-1}'' + \mathrm{Pr}Le\sum_{k=0}^{m-1} f_{m-1-k}\phi_k' + \frac{Nt}{Nb}\theta_{m-1}''\\ &- \mathrm{Pr}Le\beta_c\sum_{k=0}^{m-1} f_{m-1-k} f_{k-1}'\phi_k'\\ &- \mathrm{Pr}Le\beta_c\sum_{k=0}^{m-1} f_{m-1-k} f_{k-1}\phi_k''\\ &- \beta_c\frac{Nt}{Nb}\sum_{k=0}^{m-1} f_{m-1-k}\theta_k''\end{aligned}\right\}, \quad (23)$$

$$\chi_m = \begin{cases}0, & m \leqslant 1\\ 1, & m > 1\end{cases}. \quad (24)$$

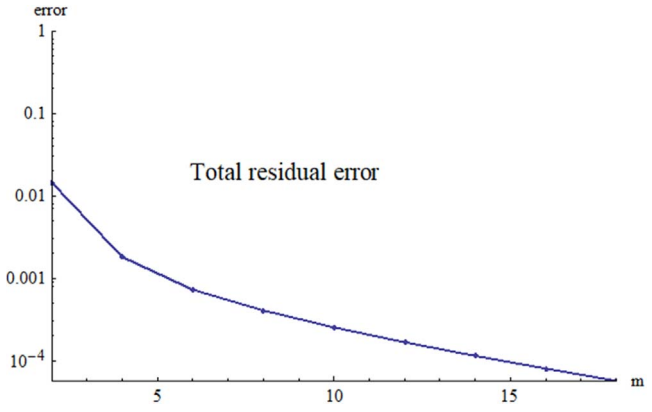

Figure 2. Total residual error.

5. Convergence analysis

Average squared residual error minimization for convergent solutions were given by Liao [27]

$$\varepsilon_m^f = \frac{1}{k+1}\sum_{k}^{i=0}\left[N_f\left(\sum_{j=0}^{m} f(\zeta)\right)_{\eta=i\delta\eta}\right]^2, \quad (25)$$

$$\varepsilon_m^\theta = \frac{1}{k+1}\sum_{i=0}^{k}\left[N_\theta\left(\sum_{j=0}^{m} f(\zeta),\ \sum_{j=0}^{m}\theta(\zeta)\right)_{\eta=i\delta\eta}\right]^2, \quad (26)$$

$$\varepsilon_m^\phi = \frac{1}{k+1}\sum_{k}^{i=0}\left[N_\phi\left(\sum_{m}^{j=0} f(\zeta),\ \sum_{m}^{j=0} g(\zeta),\ \sum_{m}^{j=0}\phi(\zeta)\right)_{\eta=i\delta\eta}\right]^2, \quad (27)$$

Total squared residual error is [27]:

$$\varepsilon_m^t = \varepsilon_m^f + \varepsilon_m^\theta + \varepsilon_m^\phi, \quad (28)$$

in which ε_m^t denotes total squared residual error.

Graphically, Total squared residual error is calculated in figure 2. Table 1 is prepared to demonstrate the individual averaged squared residual errors versus the convergence control variables.

Table 1 represents the total residual error analysis for the momentum, temperature and concentration equations. Table 2 highlights the comparative examination of the present outcomes with Pop *et al* [28] and Sharma and Singh [27] and found very interesting similarity results with each other.

6. Discussion

Here we employed OHAM to develop the convergent solutions for nonlinear system. Salient characteristics of velocity, concentration and temperature are discussed. Surface drag force, gradient of temperature and heat transfer rate are numerically calculated.

Table 1. Numerical iteration for individual averaged squared residual errors.

m	ε_m^f	ε_m^θ	ε_m^ϕ
2	0.00342246	0.00106316	0.0100455
6	4.69669×10	0.0000365382	0.000683542
10	2.70621×10	1.95932×10	0.000250546
12	1.99284×10	4.35915×10	0.000166162
16	1.44111×10	2.49058×10	0.0000797267
18	9.70307×10	1.3687×10	0.0000565754

Table 2. Obtained results accuracy analysis with Pop *et al* [28] and Sharma and Singh [27].

A	Pop *et al* [28]	Sharma and Singh [27]	Present outcomes
0.1	−0.9694	−0.9694	−0.96939
0.2	−0.9181	−0.9181	−0.91811
0.5	−0.6673	−0.6673	−0.66726

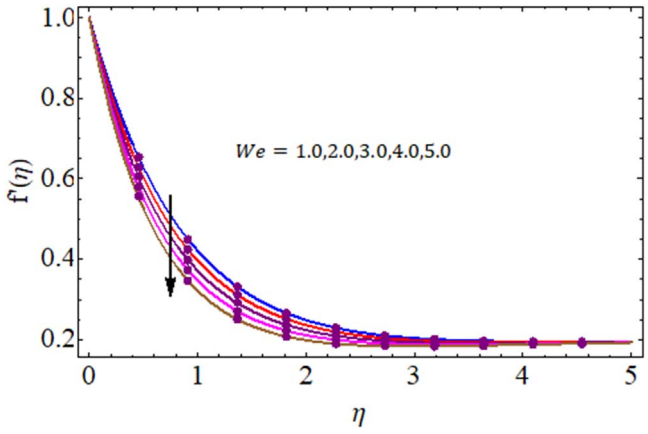

Figure 3. Velocity field versus *We*.

6.1. Velocity field

Salient features of Weissenberg number, magnetic parameter and velocity ratio parameter or stretching ratio parameter are scrutinized in figures (3–5). Characteristics of Weissenberg number on the velocity field is demonstrated in figure 3. It is seen that an increments in Weissenberg number lead to decay of velocity. Physically, for rising estimation of Weissenberg number, the relaxation time of material boosts which resists the fluid particles motion and as a result velocity of the particles declines. Figure 4 interpreted the performance of magnetic parameter on the velocity distribution. Clearly, the

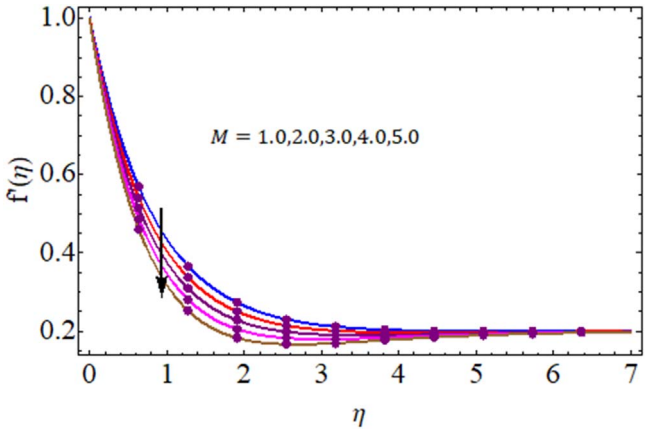

Figure 4. Velocity field versus *M*.

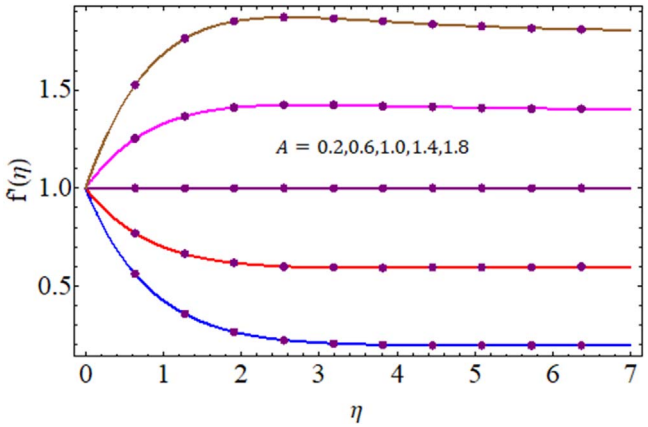

Figure 5. Velocity field versus *A*.

curves of velocity field declines against larger magnetic parameter. Physically, magnetic field associated with Lorentz force and for increasing estimation of magnetic parameter the Lorentz force increasing which resists the fluid velocity directly. That's why the velocity field diminishes. Figure 5

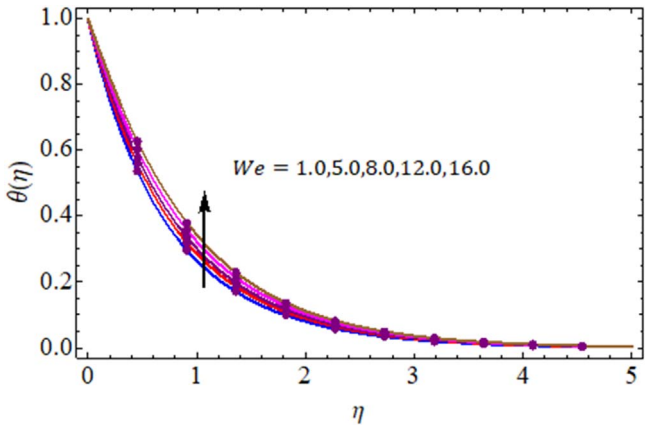

Figure 6. Temperature field versus *We*.

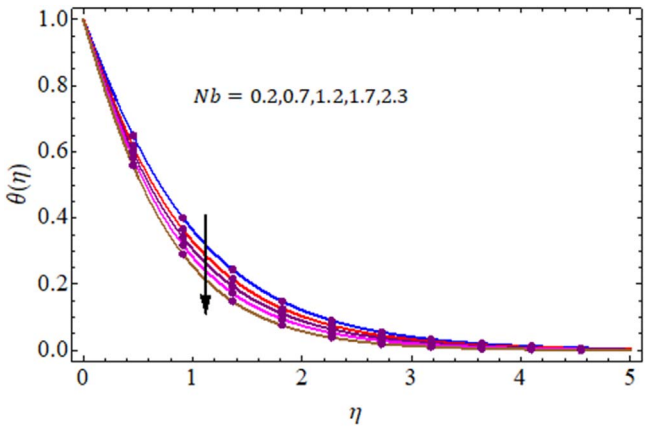

Figure 9. Temperature field versus *Nb*.

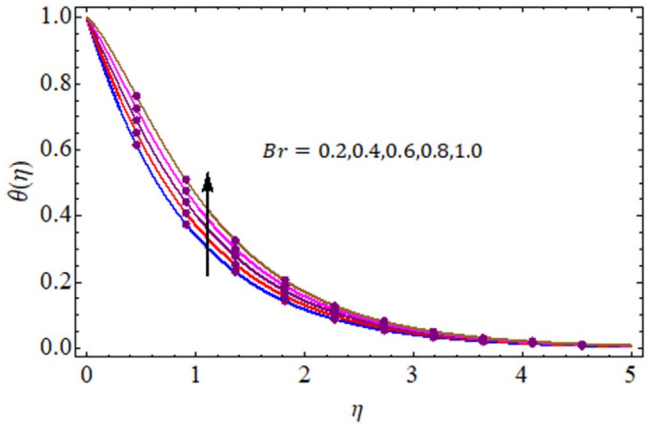

Figure 7. Temperature field versus *Br*.

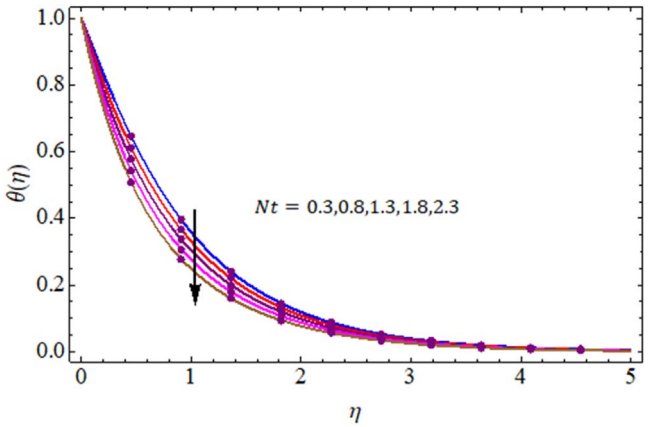

Figure 10. Temperature field versus *Nt*.

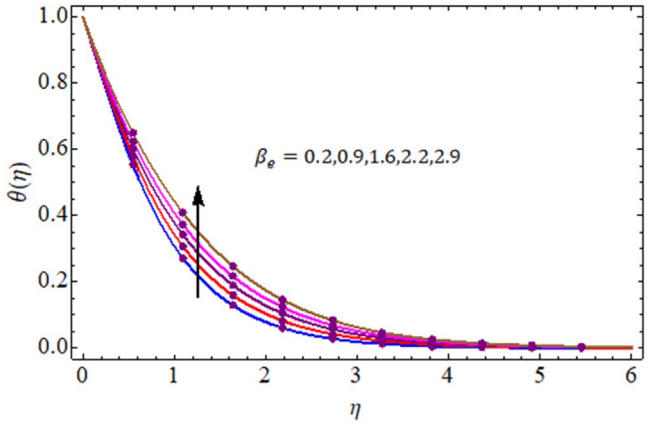

Figure 8. Temperature field versus β_e.

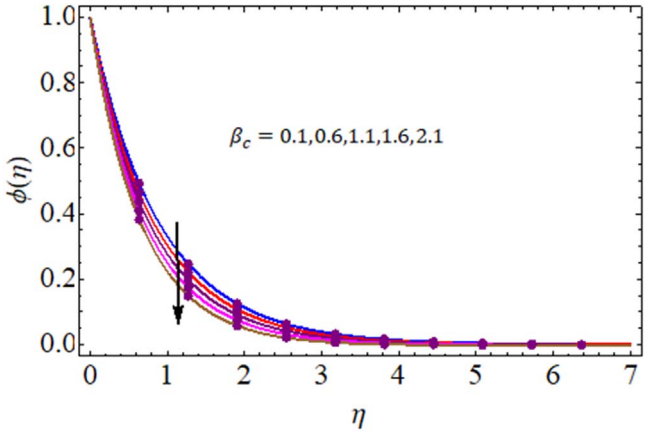

Figure 11. Concentration field versus β_c.

demonstrated the salient aspects of velocity ratio on the velocity profile. Here, three different cases of boundary layer exists for the velocity ratio parameter. Case 1: there no boundary layer formation exists for $A = 1$, because both sheet and fluid particles moves with the same velocity. Case 2: when $A > 1$, the sheet and fluid particles moves with different velocity and the velocity of particles is more than the sheet velocity. Case 3: $A < 1$, the velocity of sheet is more than the material particles means fluid particles.

6.2. Temperature field

This subsection discusses the impacts of Weissenberg number, Brinkman number, thermal relaxation time parameter, Brownian motion variable, solutal relaxation time variable and thermophoresis parameter on the temperature field. Figure 6 depicts behavior of Weissenberg number on the temperature field. Here temperature is more against higher values of Weissenberg number. Physically, for increasing the

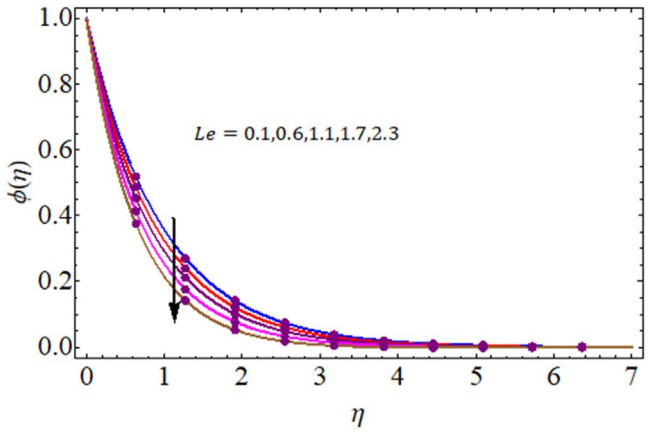

Figure 12. Concentration field versus *Le*.

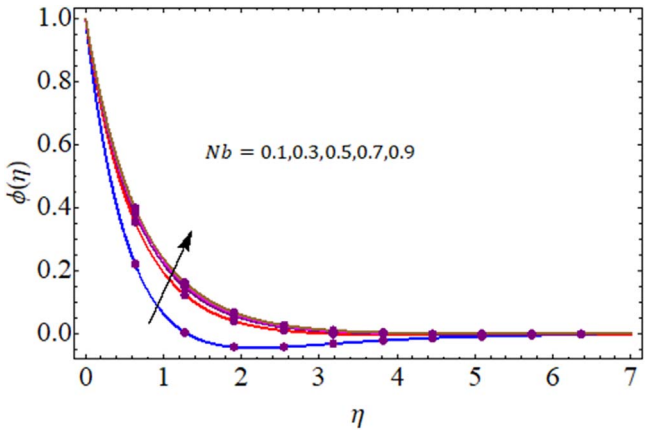

Figure 14. Concentration field versus *Nb*.

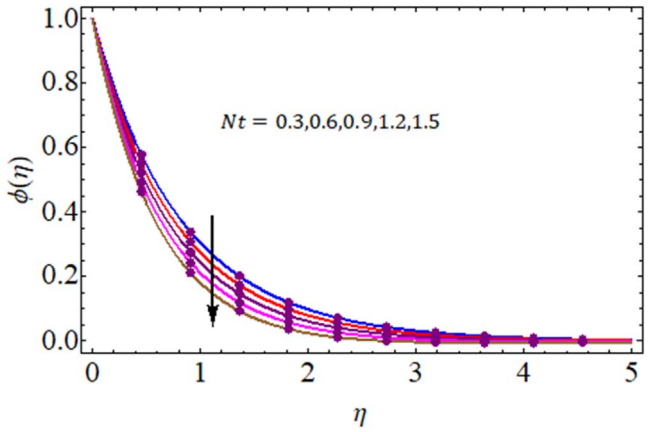

Figure 13. Concentration field versus *Nt*.

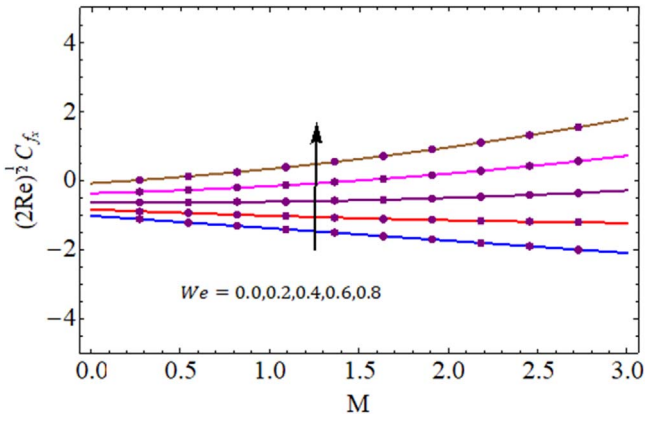

Figure 15. Skin friction coefficient analysis versus *We* and *M*.

values of Weissenberg number, the stretching rate boosts and as a result more disturbance occur in the working fluid due to which the temperature of the fluid particles increases. Figure 7 demonstrates the behavior of Brownian motion variable on the temperature profile. Less heat conduction is created by dissipation and therefore temperature profile boosts for rising Brownian motion parameter. Figure 8 displayed relaxation parameter due to temperature influence on thermal field. Here, temperature field and associated layer are decreasing functions of thermal relaxation variable. Physically, for rising thermal relaxation variable, more time is required to transfer into the neighboring nanoparticles and consequently temperature of fluid particles diminishes. Figures 9 and 10 are plotted to judge the impact of Brownian motion variable and thermophoretic parameter on the temperature field. Here both temperature and associated thermal layer thickness declines versus higher values of both Brownian motion parameter and thermophoretic variable.

6.3. Concentration

Characteristics of solutal relaxation parameter on the nanoparticle concentration has been elaborated in figure 11. Clearly, the nanoparticle concentration field is decreasing function of solutal relaxation parameter. In physical point of view, for higher values of solutal relaxation parameter, the particles of the working fluid needs more time to diffuse which yields reduction in nanoparticle concentration profile. Figure 12 displays behavior of Lewis number on nanoparticle concentration field. Here higher approximation of Lewis number give rise to decay of nanoparticle concentration. Influence of nanoparticle concentration against Brownian motion variable and thermophoretic diffusion are highlighted in figures 13 and 14. As anticipated, the nanoparticle concentration boosts against higher values of both pertinent parameters i.e., Brownian motion and thermophoretic diffusion parameter. It is also remarked that the solutal concentration boundary layer also upsurges versus these two parameters.

6.4. Engineering quantities

Significant effects of different interesting parameter on skin friction coefficient (C_{fx}) are deliberated through graphs.

6.4.1. Skin friction coefficient. Here physical characteristics of magnetic parameter and Weissenberg number on the skin friction coefficient is demonstrated in figure 15. As expected, the magnitude of skin friction coefficient boost against higher Weissenberg number and fixed values of magnetic parameter. Physically, for rising Weissenberg number, the viscosity of

the working fluid declines and as a result less friction produce between the stretched surface and fluid particles and therefore the magnitude of skin friction coefficient boosts.

7. Conclusions

The current communication highlights Cattaneo-Christov heat and mass fluxes in magnetohydrodynamic stagnation point flow of Williamson nano-liquid. Main conclusions are given below.

- Velocity decreases for larger approximations of (We) and (M).
- ($f'(\eta)$) increases against higher (A).
- Variation of Weissenberg number (We) yields improvement of ($\theta(\eta)$).
- (β_e) and (β_c) have opposite impacts on temperature.
- ($\theta(\eta)$) is decreased versus (Nt) and (Nb).
- Reverse effect of concentration is seen against (Nt) and (Nb).
- ($\phi(\eta)$) decreases when (Le) enhances.
- ($\phi(\eta)$) is increased against higher (β_c).
- Skin friction coefficient boosts up for (M) and (We).

Acknowledgments

Not applicable

Availability of data and materials

The data that support the findings of this study are available within the article; the data are made by the authors themselves and do not involve references of others.

Competing interests

The author declared that it has no conflict of interest.

Funding

Not applicable

Author contributions

Not applicable

ORCID iDs

M Ijaz Khan https://orcid.org/0000-0003-2036-0372

References

[1] Cattaneo C 1949 Sulla conduzione del calore *Atti Sem. Mat. Fis. Univ. Modena* **3** 83–101
[2] Hayat T, Farooq M, Alsaedi A and Al-Solamy F 2015 Impact of Cattaneo-Christov heat flux in the flow over a stretching sheet with variable thickness *AIP Adv.* **5** 087159
[3] Khan S U, Shehzad S A and Ali A 2018 Interaction of magneto-nanoparticles in Williamson fluid flow over convective oscillatory moving surface *Journal of the Brazilian Society of Mechanical Sciences and Engineering* **40** 195
[4] Zhang Y, Yuan B, Bai Y, Cao Y and Shen Y 2018 Unsteady Cattaneo-Christov double diffusion of Oldroyd-B fluid thin film with relaxation-retardation viscous dissipation and relaxation chemical reaction *Powder Technol.* **338** 975–82
[5] Farooq M, Ahmad S, Javed M and Anjum A 2017 Analysis of Cattaneo-Christov heat and mass fluxes in the squeezed flow embedded in porous medium with variable mass diffusivity *Results in Physics* **7** 3788–96
[6] Waqas M, Khan M I, Hayat T, Alsaedi A and Khan M I 2017 On Cattaneo-Christov double diffusion impact for temperature-dependent conductivity of Powell-Eyring liquid *Chin. J. Phys.* **55** 729–37
[7] Hayat T, Khan M I, Farooq M, Alsaedi A, Waqas M and Yasmeen T 2016 Impact of Cattaneo-Christov heat flux model in flow of variable thermal conductivity fluid over a variable thicked surface *Int. J. Heat Mass Transfer* **99** 702–10
[8] Upadhay M S, Mahesha and Raju C S K 2017 Cattaneo-Christov on heat and mass transfer of unsteady Eyring Powell dusty nanofluid over sheet with heat and mass flux conditions *Informatics in Medicine Unlocked* **9** 76–85
[9] Hayat T, Qayyum S, Shehzad S A and Alsaedi A 2017 Cattaneo-Christov double-diffusion model for flow of Jeffrey fluid *Journal of the Brazilian Society of Mechanical Sciences and Engineering* **39** 4965–71
[10] Malik R, Khan M, Shafiq A, Mushtaq M and Hussain M 2017 An analysis of Cattaneo-Christov double-diffusion model for Sisko fluid flow with velocity slip *Results in Physics* **7** 1232–7
[11] Choi S U S and Eastman J A 1995 Enhancing thermal conductivity of fluids with nanoparticles *ASME Publications-Fed* **231** 99–106
[12] Modak M, Chougule S S and Sahu S K 2018 An experimental investigation on heat transfer characteristics of hot surface by using CuO-water nanofluids in circular jet impingement cooling *J. Heat Transfer* **140** 012401
[13] Buongiorno J 2006 Convective transport in nanofluids *ASME Journal of Heat Transfer* **128** 240–50
[14] Hayat T, Khan S A, Khan M I and Alsaedi A 2019 Impact of activation energy in nonlinear mixed convective chemically reactive flow of third grade nanomaterial by a rotating disk *Int. J. Chem. Reactor Eng.* **17** 20180170
[15] Khan M I, Alzahrani F, Hobiny A and Ali Z 2020 Fully developed second order velocity slip Darcy-Forchheimer flow by a variable thicked surface of disk with entropy generation *Int. Commun. Heat Mass Transfer* **117** 104778
[16] Khan M, Salahuddin T and Malik M Y 2018 An immediate change in viscosity of Carreau nanofluid due to double stratified medium: application of Fourier's and Fick's laws *Journal of the Brazilian Society of Mechanical Sciences and Engineering* **40** 457
[17] Haq F, Kadry S, Chu Y M, Khan M and Khan M I 2020 Modeling and theoretical analysis of gyrotactic microorganisms in radiated nanomaterial Williamson fluid

with activation energy *Journal of Materials Research and Technology* **9** 10468–77
[18] Khan M, Malik M Y, Salahuddin T and Hussian A 2018 Heat and mass transfer of Williamson nanofluid flow yield by an inclined Lorentz force over a nonlinear stretching sheet *Results in Physics* **8** 862–8
[19] Khan M I, Kadry S, Chu Y M, Khan W A and Kumar A 2020 Exploration of Lorentz force on a paraboloid stretched surface in flow of Ree-Eyring nanomaterial *Journal of Materials Research and Technology* **9** 10265–75
[20] Khan M, Salahuddin T, Malik M Y and Mallawi F O 2018 Change in viscosity of Williamson nanofluid flow due to thermal and solutal stratification *Int. J. Heat Mass Transfer* **126** 941–8
[21] Khan M I, Alzahrani F, Hobiny A and Ali Z 2020 Estimation of entropy generation in Carreau-Yasuda fluid flow using chemical reaction with activation energy *Journal of Materials Research and Technology* **9** 9951–64
[22] Khan M, Shahid A, Malik M Y and Salahuddin T 2018 Thermal and concentration diffusion in Jeffery nanofluid flow over an inclined stretching sheet: a generalized Fourier's and Fick's perspective *J. Mol. Liq.* **251** 7–14
[23] Muhammad R, Khan M I, Khan N B and Jameel M 2020 Magnetohydrodynamics (MHD) radiated nanomaterial viscous material flow by a curved surface with second order slip and entropy generation *Comput. Methods Programs Biomed.* **189** 105294
[24] Khan M, Salahuddin T, Malik M Y, Tanveer A, Hussian A and Alqahtani A S 2020 3D axisymmetric Carreau nanofluid flow near the Homann stagnation region along with chemical reaction: application Fourier's and Fick's laws *Math. Comput. Simul* **170** 221–35
[25] Muhammad R, Khan M I, Jameel M and Khan N B 2020 Fully developed Darcy-Forchheimer mixed convective flow over a curved surface with activation energy and entropy generation *Comput. Methods Programs Biomed.* **188** 105298
[26] Idrees M, Islam S, Tirmizia S I A and Haq S 2012 Application of the optimal homotopy asymptotic method for the solution of the Korteweg–de Vries equation *Math. Comput. Modell.* **55** 1324–33
[27] Sharma P R and Singh G 2009 Effects of variable thermal conductivity and heat source/sink on MHD flow near a stagnation point on a linearly stretching sheet *Journal of Applied Fluid Mechanics* **2** 13–21
[28] Pop S R, Grosan T and Pop I 2004 Radiation effects on the flow near the stagnation point of a stretching sheet *Z. Angew. Math. Phys.* **25** 100–6
[29] Khan M, Salahuddin T, Malik M Y and Khan F 2020 Change in internal energy of Carreau fluid flow along with Ohmic heating: a Von Karman application *Physica. A* **547** 123440
[30] Khan M I, Waqas M, Hayat T and Alsaedi A 2017 A comparative study of Casson fluid with homogeneous-heterogeneous reactions *J. Colloid Interface Sci.* **498** 85–90